

Comptonization in the vicinity of black hole horizon

Andrzej Niedźwiecki,

Lódz University, Department of Physics, Pomorska 149/153, 90-236 Lódz, Poland

29 September 2004

ABSTRACT

Using a Monte Carlo method, we derive spectra arising from Comptonization taking place close to a Kerr black hole. We consider a model consisting of a hot thermal corona Comptonizing seed photons emitted by a cold accretion disc. We find that general relativistic effects are crucial for the emerging spectra in models which involve significant contribution of radiation produced in the black hole ergosphere. Due to this contribution, spectra of hard X-ray emission produced in the vicinity of a rapidly rotating black hole strongly depend on the inclination of the line of sight, with larger inclinations corresponding to harder spectra. Remarkably, such anisotropy could be responsible for properties of the X-ray spectra of Seyfert galaxies, which appear to be intrinsically harder in type 2 objects than in type 1, as reported recently.

Key words: accretion, accretion discs – radiation mechanisms: thermal – X-rays: binaries.

1 INTRODUCTION

A large fraction of the energy liberated by accretion onto black holes is released in an optically thin plasma, which produces hard X-rays by Compton upscattering of soft photons. In some cases this hard X-ray source must be located in the immediate vicinity of a black hole, as indicated by Fe K α emission line profiles revealed by *Chandra* and *XMM-Newton* (e.g. Wilms et al. 2001; Miller et al. 2002). If those lines are produced at inner accretion discs, their steep radial emissivities require illumination by hard X-rays to be centrally concentrated within a few gravitational radii, which in turn implies that the X-rays are generated close to the black hole horizon. In such cases the X-ray spectra should be affected by Doppler and gravitational energy shifts as well as ray bending effects. The influence of strong gravity on Compton scattering expresses itself in an extreme way in the ergosphere, where scatterings can extract rotational energy of a black hole (Piran & Shaham 1977a).

Despite the expected importance of these effects, there has been little work done to investigate their impact on Comptonization spectra emerging from black hole accretion flows. Piran & Shaham (1977b) considered production of γ -rays in the black hole ergosphere by Compton upscattering of X-ray photons. However, their results do not have a form suitable to compare them with current observations of black hole systems. We find also that their conclusions are partially incorrect. More recently, Comptonization in advection-dominated accretion flows around Kerr black holes has been analyzed by Kurpiewski & Jaroszyński (1999) and Manmoto

(2000). However, emission from such flows is dominated by radiation produced in regions rather distant from a black hole, where effects of strong gravity are not significant, as we find in this paper. Laurent & Titarchuk (1999) derived spectra of Comptonization on a relatively cold plasma moving with relativistic velocities close to a black hole. However, these bulk motion Comptonization models have assumed so far only the Schwarzschild metric, omitting processes taking place in the ergosphere, where strong gravity effects are most prominent.

In this paper we study formation of Comptonization spectra using a fully general relativistic description of photon transfer and Compton scatterings in a plasma located close to a Kerr black hole. For our investigation we choose a model in which seed photons are emitted by a cold disc, while Comptonization takes place in a hot thermal corona. We derive the cold disc emission and the Comptonization spectra by following individual photon trajectories. We use a Monte Carlo method to simulate both the thermal emission of the disc and Compton scatterings.

We take into account two geometries of a disc-corona system which are popular in modeling the central part of black hole accretion flows. Firstly, we consider a model involving inner corona replacing a cold disc in the central region. This geometry is similar to solutions with a hot optically thin flow existing in the inner part of a cold disc (e.g. Shapiro, Lightman & Eardley 1976; Narayan & Yi 1995; Esin, McClintock & Narayan 1997), although we assume a much lower distance of transition between the disc and the inner corona than in standard versions of this solution. Sec-

ondly, we consider a corona surrounding a cold disc, corresponding to models of a hot dissipative corona formed on top of the disc surface (e.g. Liang & Price 1977; Haardt & Maraschi 1991).

In Section 2 we describe details of our model. In Section 3 we analyze relevant relativistic effects. Examples of our model spectra are shown in Section 4. We discuss our results in Section 5 and summarize our conclusions in Section 6.

2 MODEL DESCRIPTION

2.1 Geometry and model parameters

We consider a Kerr black hole accreting matter at a mass accretion rate \dot{M} . The black hole is characterized by its mass, M , and angular momentum, J . We use the Boyer-Lindquist (BL) coordinate system $x^i = (t, R, \theta, \phi)$. The metric tensor components, g_{ij} , are given, e.g., in Bardeen, Press & Teukolsky (1972). We also make use of locally non-rotating (LNR) frames (Bardeen et al. 1972), which are particularly convenient for studying processes in the Kerr geometry.

The following dimensionless parameters are used in the paper

$$r = \frac{R}{R_g}, \quad \hat{t} = \frac{ct}{R_g}, \quad \dot{m} = \frac{\dot{M}}{\dot{M}_{\text{Edd}}}, \quad a = \frac{J}{cR_g M}, \quad \Omega = \frac{d\phi}{dt},$$

where $\dot{M}_{\text{Edd}} = 4\pi GMm_p/(\sigma T c)$ is the Eddington accretion rate and $R_g = GM/c^2$ is the gravitational radius. Inclination of the rotation axis of the black hole to the line of site is given by $\mu_{\text{obs}} \equiv \cos \theta_{\text{obs}}$. We focus on black holes characterized by the highest expected value of the spin parameter, $a = 0.998$ (Thorne 1974). Such black holes are referred to in this paper as maximally rotating. Processes taking place in the ergosphere, which is a region contained within the surface given by $R_{\text{erg}} = R_g[1 + (1 - a^2 \cos^2 \theta)^{1/2}]$ but outside the event horizon, appear particularly important for our study.

We assume that the accreting material forms a geometrically thin, optically thick disc and that a hot coronal region exists in the neighborhood of the innermost part of the disc. We consider two models of a disc-corona system:

- (i) an inner corona replacing a cold disc inside some transition radius, r_{tr} ;
- (ii) a cold disc extending down to the black hole horizon with a hot corona formed above the surface of the innermost disc; the radius of a region covered by the corona in this model is denoted as r_c .

We focus our investigation on the impact of strong gravity effects on formation of spectra rather than on a precise modeling of a disc-corona system. Therefore, we make a number of simplifying assumptions in our model.

We follow standard description for a geometrically thin disc (e.g. Novikov & Thorne 1973), assuming that the disc rotates in the equatorial plane of the Kerr geometry with Keplerian angular velocity (Bardeen et al. 1972),

$$\Omega_K(r) = \frac{1}{a + r^{3/2}}, \quad (1)$$

and that it emits released energy as blackbody radiation with the surface brightness distribution described by the standard formula given by Page & Thorne (1974). For a disc extending down to the black hole [model (ii)] there is

no emission below the marginally stable orbit, located at $r_{\text{ms}} = 1.23$ for $a = 0.998$.

In our model of a corona we assume that hot electrons have Maxwellian distribution of energy in the corona rest frame; that the corona is isothermal; and that the coronal material corotates with the disc (except for model B defined below) with no transversal or radial motion, $u^\theta = 0$ and $u^r = 0$.

While corotation of the hot plasma with the disc seems natural for a model with corona formed above the disc surface, velocity field in the inner corona is an uncertain issue. However, hydrodynamical studies typically indicate that in the extreme Kerr metric the region where radial velocity becomes relativistic is very narrow, which supports our approximation of the velocity field by a quasi-Keplerian motion.

In particular, solutions of advection-dominated accretion flows (Popham & Gammie 1998; Manmoto 2000) indicate that for a rapidly rotating black hole accretion proceeds with a rather low radial velocity even close to the event horizon (while for slowly rotating black holes rapid acceleration of the flow occurs at further distances). Although these results are not directly applicable to our model as they are based on assumption that a quasi-spherical flow is formed far from a black hole, they confirm that fast rotation of a black hole stabilizes rotationally supported flows. Specifically, for $a = 0.998$ these models typically yield radial velocity increasing from $0.3c$ at $r = 2$ to $0.7c$ at $r = 1.2$. Emission of accretion flows with such velocities differs from emission of a Keplerian flow mainly by increased fraction of photons captured by black hole (see Section 3.2). Then, overestimated strength of emission from the ergospheric region is a major shortcoming due to neglect of radial velocity in modeling spectra of such flows.

Even stronger support for our model comes from the MHD simulations, which do not reveal formation of any significant sub-Keplerian component. In simulations with $a = 0.998$ a quasi-Keplerian torus extends deep into the ergosphere and the plunging region is extremely narrow (the radial velocity profile on Figure 12 in De Villiers, Hawley & Krolik 2003 shows velocity smaller than $0.1c$ at r_{ms}).

On the other hand, our description of the accretion flow is not appropriate for investigation of spectra produced by strongly sub-Keplerian flows, which are postulated in models considering Comptonization dominated by transfer of kinetic energy from bulk motion of such a flow (e.g. Chakrabarti & Titarchuk 1995, Laurent & Titarchuk 1999). We make a thorough study of spectra arising from such relativistic inflows in a separate paper, extending formalism developed here by a proper treatment of the propagation of photons in a plasma with high radial velocity.

Velocity of the corona rest frame relative to the LNR frame and corresponding Lorentz factor are related to angular velocity, $\Omega(r, \theta)$, by (Bardeen et al. 1972)

$$V \equiv \frac{v^\phi}{c} = \frac{\sin \theta A}{\Sigma \Delta^{1/2}} (\Omega - \omega), \quad \Gamma_{\text{ln}} = [1 - V^2]^{-1/2}, \quad (2)$$

where

$$\Delta = r^2 - 2r + a^2, \quad \Sigma = r^2 + a^2 \cos^2 \theta,$$

$$A = (r^2 + a^2)^2 - a^2 \Delta \sin^2 \theta, \quad \omega = 2ar/A. \quad (3)$$

The rest density of electrons in the corona, n , is described by a dimensionless parameter,

$$\hat{n} = nR_g\sigma_T, \quad (4)$$

where σ_T is the Thomson cross-section.

The following assumptions on distributions of the rest density and angular velocity define three specific models of the corona.

Model A: a spherical corona. This model assumes that the distribution of rest density is uniform, $\hat{n} = \text{const}$, in a sphere with radius r_{tr} for model (i) and r_c for model (ii), and that the angular velocity is constant on spheres, with

$$\Omega(r, \theta) = \Omega_K(r). \quad (5)$$

Model B: a non-rotating spherical corona. This model adopts the same assumptions as model A except for angular velocity which is set to be equal to the velocity of the LNR observer, $\Omega = \omega$, yielding $V \equiv 0$.

Model C: a slab-like corona. This model assumes that angular velocity distribution is given by

$$\Omega(r, \theta) = [a + (r \sin \theta)^{3/2}]^{-1} \quad (6)$$

and that the corona fills only a region within 12° from the equatorial plane. The latter assumption is due to the fact that angular velocity given by equation (6) violates the causality condition, $g_{tt} + 2g_{t\phi}\Omega + g_{\phi\phi}\Omega^2 < 0$, at high latitudes. In this model we assume also that the rest density decreases with radius as $\hat{n} \propto r^{-1}$, which gives approximately constant vertical optical depth of the corona.

Most of our model spectra, in both geometries of a disc-corona system, are computed for a spherical corona model A. Spectra of discs sandwiched by coronae described by models B and C are presented in Section 4.2 to illustrate influence of assumed velocity field and density distribution on spectral properties.

We do not attempt to model a region where the flow accelerates inward to relativistic velocities. As discussed above, this region should be very narrow and its emission is very unlikely to give any noticeable contribution to observed spectrum. Specifically, we neglect the region inside $r_{\text{min}} = 1.13$, where approximation by a Keplerian motion would yield artificially high orbital velocity ($V > 0.6$, approaching the speed of light at the prograde circular photon orbit located at $r_{\text{ph}} = 1.07$). We have checked that spectra presented in this paper are weakly (in most cases negligibly) sensitive on the choice of any specific value of r_{min} close to r_{ms} . The most significant change of spectrum due to the change of this parameter occurs for edge-on spectrum in Fig. 9(a), which has a strong contribution of emission from deep regions of the ergosphere (spectra obtained with $r_{\text{min}} = 1.13$ and 1.23 are compared in that figure).

2.2 Photons in the Kerr geometry

We summarize here relevant properties of photon motion in the Kerr metric. A photon trajectory is determined by two dimensionless constants of motion

$$\eta \equiv \frac{Qc^2}{E_{\text{inf}}^2 R_g^2}, \quad \lambda \equiv \frac{Lc}{E_{\text{inf}} R_g}, \quad (7)$$

where E_{inf} is the photon energy at infinity, Q is the Carter's constant, L is the component of angular momentum paral-

lel to the black hole rotation axis. The following equations govern the photon trajectory (e.g. Bardeen et al. 1972)

$$\begin{aligned} \frac{d\hat{t}}{d\zeta} &= \frac{A(1 - \omega\lambda)}{\Sigma\Delta}, \quad \frac{dr}{d\zeta} = \pm \frac{R^{1/2}}{\Sigma}, \quad \frac{d\theta}{d\zeta} = \pm \frac{\Theta^{1/2}}{\Sigma}, \\ \frac{d\phi}{d\zeta} &= \frac{\lambda(\Sigma - 2r)}{\Sigma\Delta \sin^2 \theta} + \frac{2ar}{\Sigma\Delta}, \end{aligned} \quad (8)$$

where

$$\begin{aligned} R &= (r^2 + a^2 - \lambda a)^2 - \Delta [(\lambda - a)^2 + \eta], \\ \Theta &= \eta + \cos^2 \theta (a^2 - \lambda^2 / \sin^2 \theta), \end{aligned} \quad (9)$$

and ζ is an affine parameter.

While photon motion is simply described in the BL coordinates, local rest frames are more appropriate for description of physical processes. Applying the transformation between the BL coordinate frame and the LNR frame, given by Bardeen et al. (1972), we find energy and momentum of a photon measured by the LNR observer

$$\begin{aligned} E_{\text{ln}} &= E_{\text{inf}} (1 - \omega\lambda) \left(\frac{A}{\Sigma\Delta} \right)^{1/2}, \quad p_{(\phi)} = \frac{E_{\text{inf}}}{c} \frac{\lambda}{\sin \theta} \left(\frac{\Sigma}{A} \right)^{1/2}, \\ p_{(\theta)} &= \pm \frac{E_{\text{inf}}}{c} \left(\frac{\Theta}{\Sigma} \right)^{1/2}, \quad p_{(r)} = \pm \frac{E_{\text{inf}}}{c} \left(\frac{R}{\Sigma\Delta} \right)^{1/2}. \end{aligned} \quad (10)$$

Then, a Lorentz transformation yields the energy and momentum in the rest frame of the plasma. In particular, photon energy in the rest frame

$$E_{\text{rest}} = \Gamma_{\text{ln}} (E_{\text{ln}} - v^\phi p_{(\phi)}). \quad (11)$$

Putting in the above equations velocity of a Keplerian disc, $v^\phi = V_K \equiv (\Omega_K - \omega)A/(\Sigma\Delta^{1/2})$, we find direct relations (given in a similar form by Bardeen & Cunningham 1973) between the constants of motion of a photon, λ , η and E_{inf} , and its energy and directional angles measured in the disc rest frame

$$\begin{aligned} g &\equiv \frac{E_{\text{inf}}}{E_{\text{disc}}} = \left(\frac{\Delta\Sigma}{A} \right)^{1/2} \frac{(1 - V_K^2)^{1/2}}{1 - \Omega_K \lambda}, \quad \eta = \left(\frac{r \cos \theta_{\text{em}}}{g} \right)^2, \\ \lambda &= \frac{\sin \phi_{\text{em}} \sin \theta_{\text{em}} + V_K}{\Omega_K \sin \phi_{\text{em}} \sin \theta_{\text{em}} + \Sigma\Delta^{1/2} A^{-1} + \omega V_K}, \end{aligned} \quad (12)$$

where E_{disc} is the energy in the disc rest frame, θ_{em} is the polar angle with respect to direction perpendicular to the disc surface, and ϕ_{em} is the azimuthal angle, in the disc plane, with respect to coordinate r direction.

For motion in a curved space-time we must integrate optical depth along a photon trajectory separately for each photon. The increase of the optical depth is given by $dt = \sigma(E_{\text{rest}})ndl'$, where σ is the Klein-Nishina cross-section (averaged over Maxwellian distribution of electron velocities), n is the rest density of electrons and dl' is the length along the photon path measured in the plasma rest frame. We find this length using the obvious relation, $dl' = cdt'$, where dt' is the time interval measured in the plasma rest frame which can be derived for a given trajectory as follows. Transforming the BL coordinate differentials $d\hat{t}$ and $d\phi$ to the LNR frame and then making a Lorentz transformation to the plasma rest frame we get

$$\begin{aligned} \frac{cdt'}{R_g} &= \Gamma_{\text{ln}} [(\Delta\Sigma/A)^{1/2} d\hat{t} \\ &\quad - V(A/\Sigma)^{1/2} \sin \theta (d\phi - \omega d\hat{t})]. \end{aligned} \quad (13)$$

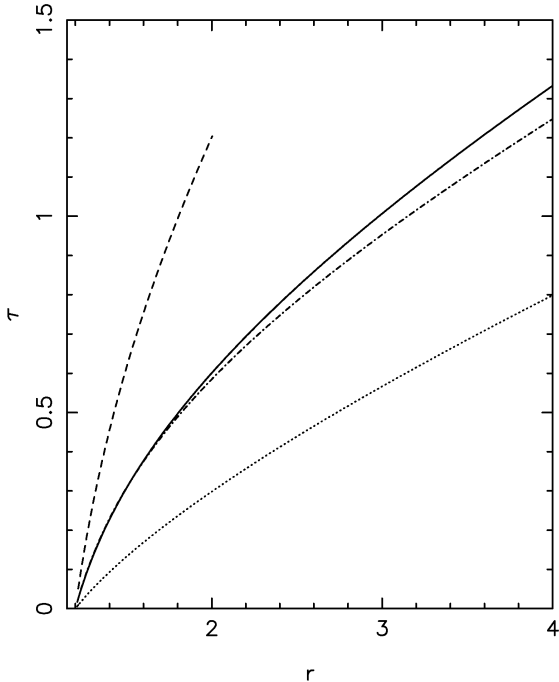


Figure 1. Optical depths along radial trajectories of outgoing photons emitted at $r = 1.2$. Solid, dotted and dashed curves correspond to trajectories in the equatorial plane of a Kerr black hole ($a = 0.998$). Dot-dashed curve is for trajectory with a constant polar angle $\theta = 0.1\pi$ (close to the polar axis). Photons propagate through a thermal plasma with $kT_e = 80$ keV and with the rest density $\hat{n} = 0.4$ for the dashed curve and $\hat{n} = 0.2$ for the remaining curves. Dotted curve is for a photon with $E_{\text{inf}} = 50$ keV, the remaining curves for $E_{\text{inf}} = 0.1$ keV. Note that the optical depth for a photon with $E_{\text{inf}} = 50$ keV is reduced by 50 per cent between $r = 1.2$ and $r = 2$ (compare dotted and solid curves).

Then, using equation (4), we obtain

$$\begin{aligned} d\tau &= \hat{n} \frac{\sigma(E_{\text{rest}})}{\sigma_T} \Gamma_{\ln} \left(\frac{\Delta\Sigma}{A} \right)^{1/2} \left[\left(1 + V \frac{2ar \sin \theta}{\Sigma \Delta^{1/2}} \right) \frac{d\hat{t}}{d\zeta} \right. \\ &\quad \left. - V \frac{A \sin \theta}{\Sigma \Delta^{1/2}} \frac{d\phi}{d\zeta} \right] d\zeta, \end{aligned} \quad (14)$$

where the derivatives $d\hat{t}/d\zeta$ and $d\phi/d\zeta$ are given by equation (8).

Note that in the ergosphere E_{rest} is typically a few times higher than E_{inf} due to the gravitational blueshift. Therefore, close to a black hole the Klein-Nishina corrections can decrease significantly the optical depth even for photons which in flat space-time would be still in the Thomson regime. Fig. 1 shows optical depths integrated along radial trajectories (characterized by $\lambda = 0$ and $p_\theta = 0$; the latter condition implies $\eta = -a^2 \cos^2 \theta$) of photons escaping from $r = 1.2$. Photons propagate through a plasma with the same temperature and rest density as assumed for models presented in Section 4. Note that the optical depth for a photon with $E_{\text{inf}} = 50$ keV is decreased by around 50 per cent in the ergosphere due to the reduction of the cross section. Then, curvature in spectra may occur at a few tens of keV (indeed seen in some spectra presented in Section 4).

Note also that assumptions underlying a spherical corona model yield similar optical depths of the corona in

different directions with respect to the symmetry axis of the system.

2.3 Monte Carlo simulation

Our procedure for computing spectra is based on the Monte Carlo method and involves calculation of many photon trajectories. A similar approach to computing spectra of black hole accretion flows was applied, e.g., by Laor, Netzer & Piran (1990), Laurent & Titarchuk (1999) and Kurpiewski & Jaroszyński (1999). The free parameters of our model are r_{tr} or r_c (depending on the disc-corona model), a , M , \dot{m} , \hat{n} and electron temperature, T_e . Note that M and \dot{m} are relevant only for the emission of the cold disc. We trace individual photon trajectories originating at the disc surface. The procedure for generation of disc photons is described in Section 2.3.1 below.

Trajectories of photons reaching the hot plasma are followed, through subsequent scatterings, according to algorithm described in Section 2.3.2. Photons reaching infinity are summed over 10 bins in μ_{obs} (from 0-0.1 to 0.9-1; μ_{obs} given for spectra in Section 4 correspond to the value in the middle of the bin). Photon transfer equations are solved down to $r_{\text{min}} = 1.13$. Photons crossing the sphere of this radius are treated as captured by the black hole.

Spectra presented in Section 4 have been obtained in Monte Carlo runs involving at least 10^8 photons scattered in the corona.

2.3.1 Thermal disc emission

The emission point, r_{em} , on the disc surface is generated according to radial emissivity, F^+ , given by Page and Thorne (1974). Consecutive photons originating from this r_{em} are generated until their summed energy exceeds some fixed value, E_{tot} , much higher than a characteristic photon energy. When E_{tot} is exceeded we generate next r_{em} .

For each photon its energy, E_{disc} , is generated from the blackbody distribution with the local surface temperature, $T_{\text{surf}} = (F^+/\sigma)^{1/4}$. The initial direction in the disc rest frame is generated with a uniform distribution in ϕ_{em} . The polar angle, θ_{em} , is generated according to angular distribution of local disc emission, with the specific intensity $I(\cos \theta_{\text{em}}) \sim 1 + 2.06\theta_{\text{em}}$ corresponding to limb darkening in electron scattering limit (see, e.g., Gierliński, Maciąłek-Niedźwiecki & Ebisawa 2001). Constants of motion, η , λ and E_{inf} , are found from equation (12). Then, we solve r and θ equations of the set of equations (8) and determine whether the photon escapes to infinity (contributing to the spectrum of the disc emission), returns to the disc (we neglected here increase of the disc temperature due to these returning photons), illuminates the corona or gets captured by the black hole.

2.3.2 Comptonization

If a photon reaches the coronal region, the optical depth is generated according to the decreasing exponential distribution $P(\tau) = e^{-\tau}$. Then, we solve equations (8) and integrate the optical depth, given by equation (14), until the trajectory crosses the horizon (see Section 2.3.3), leaves the corona

or reaches the chosen optical distance. In the last case a simulation of Compton scattering is performed as follows:

- (i) Photon momentum and energy in the plasma rest frame are found, as described in Section 2.2.
- (ii) Electron velocity is generated and scattered photon direction and energy are derived according to the procedure described in Górecki & Wilczewski (1984).
- (iii) The four-momentum of the scattered photon is Lorentz-transformed back to the LNR frame, then equations (10) are inverted for new constants of motion (E_{inf} , η , λ).

Photons leaving the corona are treated similarly to those emitted from the disc surface - considering their motion in the $r\theta$ plane we determine whether they escape from the system and contribute to the Comptonization spectrum.

3 COMPTON SCATTERING IN THE KERR METRIC

3.1 Single scattering spectra

Photons scattered in a hot corona gain energy due to both thermal motion of electrons and bulk motion of the corona. Furthermore, dynamics of individual scatterings is influenced by gravitational energy shifts. In this section we determine the range of distances from a black hole in which the gravitational effects are important for the formation of Comptonization spectra. Then, we examine qualitatively how these effects can affect the emerging spectra. For this investigation we derive spectra of a single scattering of monoenergetic photons, with initial energy E_{inf}^0 , on electrons in the Kerr geometry. We assume various distributions of electron energies to compare effects taking part in formation of the spectra. Simulation of Compton scatterings is performed according to procedure described in Section 2.3.2.

Spectra presented in this section are normalized by the number of impinging photons, $n_{\text{ph}}(E_{\text{inf}}) \equiv N(E_{\text{inf}})/N_0$, where N_0 is the number of incident photons and $N(E_{\text{inf}})$ is the number of photons observed, after scattering, at infinity with energy E_{inf} . Note that photons captured by a black hole do not contribute to the spectrum, therefore

$$\int n_{\text{ph}}(E_{\text{inf}}) dE_{\text{inf}} < 1.$$

To illustrate effects of general relativity, separated from kinematic and thermal effects, we examine first scattering on electrons at rest with respect to the LNR frame. Fig. 2(a) shows spectra for scattering of photons, with $E_{\text{inf}}^0 = 30 keV, on electrons located in the equatorial plane of a Kerr black hole. We assume that photons illuminate electrons isotropically (as seen in the LNR frame) excluding directions which correspond to negative energy, $E_{\text{inf}}^0 < 0$, of impinging photons. Also shown is the spectrum, integrated over all scattering angles, for scattering of photons with energies $E_0 = 30 keV on electrons at rest in flat space-time. For $E_0 \ll m_e c^2$ Compton scattering is nearly elastic and the spectrum emerging in flat space-time is very narrow. On the other hand, scattering in the Kerr space-time produces spectra extending remarkably further into both low and high energies. The low energy part of such spectra is a generic feature of scattering close to a black hole, resulting from the gravitational blueshift of incoming photons. Due$$

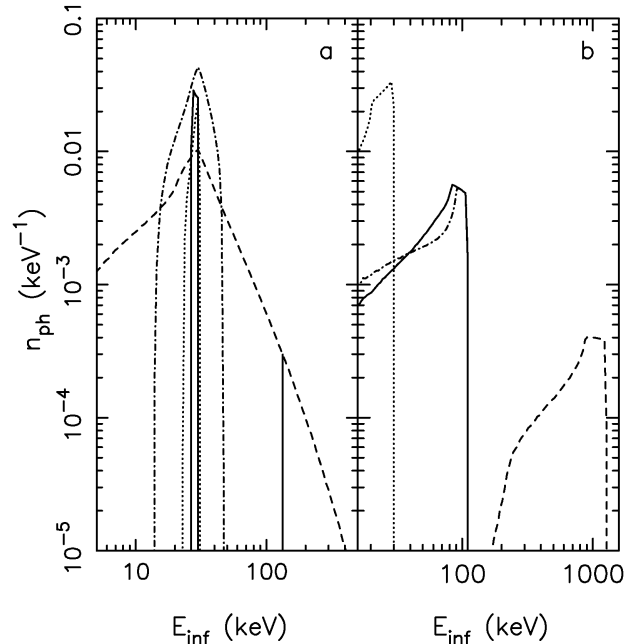


Figure 2. Angle-averaged spectra for a single scattering of photons, with $E_{\text{inf}}^0 = 30 keV, impinging on electrons at rest (with respect to the LNR frame) in the equatorial plane of the maximal Kerr geometry. (a) Photons illuminate electrons isotropically (as seen in the LNR frame). Scatterings take place at $r = 1.4$ (dashed curve), $r = 3$ (dot-dashed curve) and $r = 6$ (dotted curve). Solid curve gives the spectrum for a single scattering on electrons at rest in flat space-time, integrated over all scattering angles. The solid and dotted curves are rescaled by a factor of 0.1. Photons emerging from $r = 1.4$ with energies exceeding 135 keV (indicated by the solid vertical line) come from scatterings which extract the black hole rotational energy. (b) Dependence of the spectrum for scattering at $r = 1.4$ on the direction of impinging photons. The initial direction of photons is given by the following angles (defined in the text; $\mu_{\text{ln}} \equiv \cos \theta_{\text{ln}}$): $\mu_{\text{ln}} = 0, \phi_{\text{ln}} = \pi$ for dot-dashed curve; $\mu_{\text{ln}} = 0, \phi_{\text{ln}} = \pi/2$ for dotted curve; $\mu_{\text{ln}} = 1$ (which uniquely determines the direction) for solid curve; and $\mu_{\text{ln}} = 0.2, \phi_{\text{ln}} = 1.91\pi$ for dashed curve. Scatterings extracting the rotational energy take place only for photons impinging from the last direction.$

to this blueshift, close to a black hole photons lose in a scattering, on average, a larger amount of energy than in flat space-time.

More importantly, in the Kerr metric the relation between photon energies in the LNR frame and at infinity involves photon angular momentum, see equation (10). Therefore, the photon energy after scattering may be higher than its energy before scattering, provided that a suitable change of angular momentum occurs. Such effect is not allowed in either flat space-time or the Schwarzschild metric. The increase of photon energy can be particularly significant in the black hole ergosphere, where Penrose Inverse Compton scatterings (Piran & Shaham 1977a), for which a scattered photon has higher energy than the sum of the photon and electron energies before scattering, are permitted. Photons produced in such events form the high energy part of the spectrum, as indicated on Fig. 2(a) for the spectrum from $r = 1.4$, which extends to energies exceeding the initial energy by over an order of magnitude.

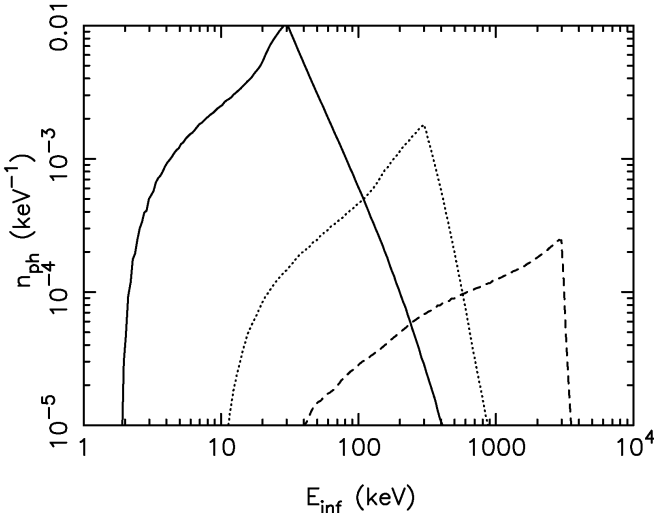


Figure 3. Angle-averaged spectra for a single scattering, at $r = 1.4$, on electrons at rest in the equatorial plane of the maximal Kerr geometry. Solid, dotted and dashed curve is for $E_{\text{inf}}^0 = 30, 300$ and 3000 keV, respectively. Photons illuminate electrons isotropically, as seen in the LNR frame.

The necessary condition for a Penrose scattering to take place is a very large blueshift of an impinging photon in the LNR frame. The blueshift is determined by the angle, Φ_{ln} , between the photon momentum and the ϕ direction in the LNR frame. Namely, using equation (10), with $p_{(\phi)} = (E_{\text{ln}}/c) \cos \Phi_{\text{ln}}$, we get

$$E_{\text{ln}} = E_{\text{inf}} (\Sigma A)^{1/2} \left(\Sigma \Delta^{1/2} + 2ar \sin \theta \cos \Phi_{\text{ln}} \right)^{-1}. \quad (15)$$

Increasingly high blueshifts correspond to narrower ranges of initial directions. E.g., for $E_{\text{inf}} = 30$ keV and $r = 1.4$, E_{ln} exceeds 100 keV for $0.45\pi < \Phi_{\text{ln}} < 0.59\pi$, while $E_{\text{ln}} > 1000$ keV for $0.58\pi < \Phi_{\text{ln}} < 0.59\pi$. Note also that strongly blueshifted photons have very large negative angular momentum ($\lambda \ll 0$) and can emerge only from a radiative process taking place in the ergosphere.

Clearly, Penrose scatterings are permitted only for certain initial directions of a photon. Fig. 2(b) illustrates dependence of the scattering spectrum on initial direction. Note that while the blueshift is determined by Φ_{ln} , different initial directions with the same Φ_{ln} give rise to different scattering spectra at infinity. The spectra in Fig. 2(b) correspond to initial directions determined in the LNR frame by the polar angle, θ_{ln} , between the photon initial direction and coordinate θ -direction, and the azimuthal angle, ϕ_{ln} , in the $r\phi$ plane, with respect to the r -direction. These angles are related to Φ_{ln} by $\cos \Phi_{\text{ln}} = \sin \phi_{\text{ln}} \sin \theta_{\text{ln}}$.

Considering possibility of generating high energy photons due to Penrose processes in black hole accretion flows, we note that a fine tuning of the initial direction is required for the most efficient scatterings and therefore probability of such events is low. Moreover, even if a photon propagates with sufficiently high blueshift in a local rest frame, probability of a scattering is strongly reduced due to the decline of the Klein-Nishina cross-section.

Fig. 3 shows dependence of the scattering spectra on initial energy of photons. The fractional loss of photon energy, in the LNR frame, increases with increasing E_{inf}^0 . There-

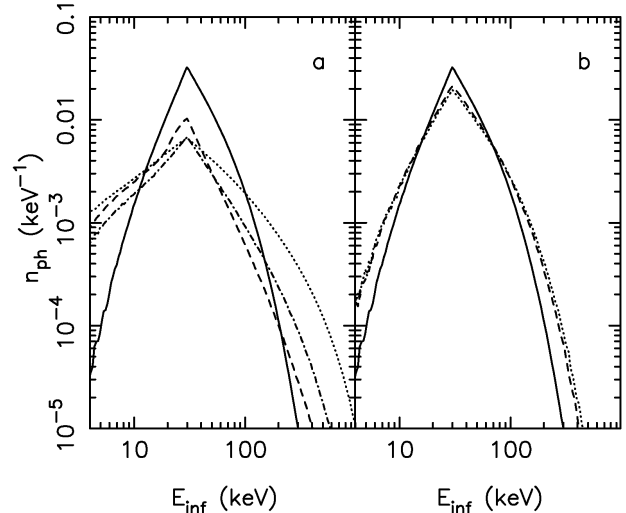


Figure 4. A spectrum for a single scattering of photons, with $E_0 = 30$ keV, on electrons with a Maxwellian distribution of velocities, $kT_e = 80$ keV, in flat space-time (given on both figures by the solid curves) compared with angle-averaged spectra for a single scattering of photons, with $E_{\text{inf}}^0 = 30$ keV, on electrons in the equatorial plane of the Kerr geometry. (a) Scattering at $r = 1.4$. Dashed curve is for scattering on cold electrons at rest in the LNR frame. Dot-dashed curve is for scattering on thermal electrons, with $kT_e = 80$ keV, at rest in the LNR frame. Dotted curve is for scattering on thermal electrons ($kT_e = 80$ keV) on a Keplerian orbit. (b) Scattering at $r = 6$ for $a = 0$ (dashed curve) and $a = 0.998$ (dotted curve). Target electrons have thermal energies ($kT_e = 80$ keV) and rotate on a Keplerian orbit. Note that difference between spectra emerging in the Schwarzschild and extreme Kerr geometries is negligible.

fore, for higher energy photons the gravitational effects are relatively less efficient in increasing photon energies.

Outside the ergosphere, the strong gravity effects are not so noticeable, as illustrated on Fig. 2(a). Photons scattered at $r = 3$ achieve energies exceeding the initial energy by up to 50 per cent and deviation of spectrum emerging from scatterings at $r = 6$ from the flat space-time scattering spectrum is insignificant. Therefore, outside the ergosphere other effects should be dominant in formation of Comptonization spectra.

Fig. 4 compares efficiency of raising the energy due to gravitational shifts with boosting of photon energies resulting from transfer of thermal and bulk motion energies of electrons. Note that the probability that a photon with $E_{\text{inf}}^0 = 30$ keV emerges with energy exceeding 100 keV after scattering on a cold electron at $r = 1.4$ is equal to that corresponding to a single scattering in a semi-relativistic thermal plasma in flat space-time. Velocity of the circular motion remains relatively low even in the deep ergosphere ($\Gamma_{\text{ln}} \lesssim 1.3$). However, combined effects of strong gravity, thermal and bulk motions may result in a large gain of energy in a single scattering, as illustrated by the dotted curve on Fig. 4(a). Then, an optically thin plasma in the ergosphere is able to generate photons with energies a few times higher than thermal energy of electrons.

Outside the ergosphere, thermal effects completely dominate. Spectrum emerging from thermal electrons in circular orbit at $r = 6$ differs only slightly from spectrum pro-

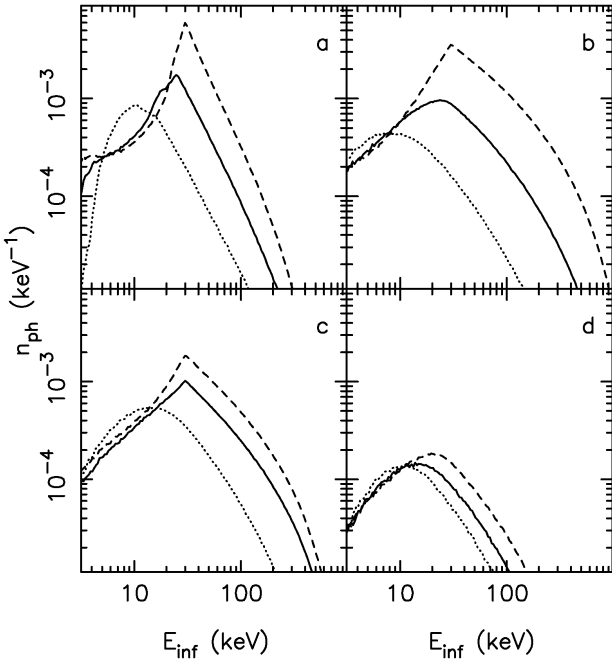


Figure 5. Spectra for a single scattering of monoenergetic photons, with $E_{\text{inf}}^0 = 30$ keV, illuminating isotropically (in the LNR frame) electrons at $r = 1.4$ in the extreme Kerr metric. Dashed, solid and dotted curves give spectra of photons scattered into $\mu_{\text{obs}} = 0 - 0.2, 0.4 - 0.6$ and $0.8 - 1$, respectively. (a) Spectra for cold electrons at rest in the equatorial plane; angle averaged spectrum is given by the dashed curve on Fig. 2(a). (b) Spectra for electrons, on a Keplerian equatorial orbit, with a Maxwellian distribution of velocities ($kT_e = 80$ keV) in the rest frame; angle averaged spectrum is given by the dotted curve on Fig. 4(a). (c) Spectra for electrons with a Maxwellian distribution of velocities ($kT_e = 80$ keV) in the rest frame. The rest of electrons rotates on a circular orbit, at $\theta = \pi/3$, with angular velocity given by equation (5). (d) Same as in Fig. 5(c) but the spectra are formed by photons which do not cross the equatorial plane after scattering.

duced by the same thermal population of electrons at rest in flat space-time [see Fig. 4(b)]. Moreover, the difference between the spectra produced, at $r = 6$, in the vicinity of a maximally rotating and a non-rotating black hole is negligible.

Fig. 5 illustrates dependence of spectra emerging from Compton scattering in the ergosphere on the inclination angle of a distant observer. Most photons emerging from the equatorial plane are observed from directions close to that plane [see Fig. 5(a)] due to the bending of photon trajectories, which is the well known effect of the Kerr geometry. Moreover, this gravitational focusing affects primarily high energy photons. As a result, spectra observed edge-on are much harder than those observed face-on. Isotropic distribution of thermal velocities of electrons does not diminish this anisotropy significantly, on the other hand circular motion further collimates radiation along the equatorial plane [see Fig. 5(b)].

Slightly more isotropic spectra come from Compton scattering taking place off the equatorial plane [see Fig. 5(c)]. Moreover, trajectories of a significant part of photons cross the equatorial plane, as illustrated by Fig. 5(d). In

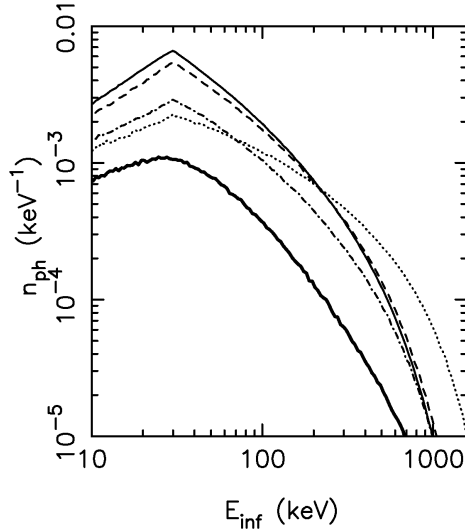


Figure 6. Angle-averaged spectra for a single scattering of monoenergetic photons, with $E_{\text{inf}}^0 = 30$ keV, on electrons with various velocities: $(v^r, v^\phi) = (0, 0.56c)$ for thinner solid curve [Keplerian flow, same as dotted curve on Fig. 4(a)]; $(-0.3c, 0.5c)$ for dashed curve; $(-0.7c, 0.36c)$ for dot-dashed curve; $(-0.9c, 0)$ for thicker solid curve; and $(-0.7c, 0.56c)$ for dotted curve. Scatterings take place at $r = 1.4$ in the equatorial plane. Isotropic illumination (in the LNR frame) of electrons and Maxwellian distribution ($kT_e = 80$ keV) of electron velocities in the rest frame are assumed.

models with an untruncated disc such photons are depleted from emerging spectra as they interact with the disc matter.

We find only a very weak anisotropy of spectra emerging from $r = 6$, regardless of the speed of black hole rotation. Then, we conclude that spectra of Comptonization in the Schwarzschild metric as well as those emerging at distances exceeding a few R_g in the Kerr metric should be correctly approximated by flat space-time Comptonization codes.

3.2 Radial velocity

Fig. 6 shows spectra for a single scattering, obtained similarly to spectra shown in Section 3.1, but for various velocity fields of Comptonizing electrons. The velocity field is parametrized by two components of velocity measured in the LNR frame: the orbital velocity, v^ϕ , and the radial velocity, v^r ($= \Delta^{-1} A^{1/2} u^r / u^t$; Bardeen et al. 1972).

The dashed and dot-dashed curves show spectra for values of v^ϕ and v^r typical for solutions of advection-dominated accretion in the ergosphere (see, e.g., Figure 1 in Popham & Gammie 1998). Clearly, scattering in a Keplerian flow (the thinner solid curve) results in the highest fraction of escaping photons. On the other hand, highest energies achieved by scattered photons are similar in both models.

We emphasize that relatively high (Keplerian) orbital velocity is essential for spectra emerging from the innermost region of accretion flow, as it collimates emission into directions for which escape to a distant observer is possible. The thicker solid and dot-dashed curves illustrate how decrease of orbital velocity affects the spectrum. Although the decrease of v^ϕ is connected with increase of v^r , yielding more efficient Doppler boosting ($\Gamma_{\text{ln}} = 1.6$ and 2.3 for the dot-

dashed and solid curve, respectively), it reduces efficiency of generating high energy photons able to escape.

Spectrum for the only velocity field producing photons more energetic than a Keplerian flow (due to both a high Lorentz factor, $\Gamma_{\text{ln}} = 2.3$, and a Keplerian orbital velocity) is shown by the dotted curve. We emphasize, however, that such a velocity field is very unlikely to describe a real flow as total specific energy in such a flow would exceed by 30 per cent its rest energy, while the opposite is expected in a dissipative flow.

We conclude that relativistic radial velocities, which can significantly increase the Doppler boosting, are allowed only in sub-Keplerian accretion flows, emission of which, however, is beamed toward the event horizon and lost.

3.3 High energy cut-off

In flat space-time, repeated scatterings of soft photons in a mildly-relativistic thermal plasma lead to formation of a power-law spectrum extending up to kT_e . Photons scattered to higher energies achieve Wien equilibrium with electrons and the spectrum has a roughly exponential turnover reflecting the thermal distribution of electron velocities. Close to a black hole this property is disturbed by energy shifts between consecutive scatterings. In particular, for photons blueshifted to energies significantly exceeding kT_e , thermal motions of electrons become less significant and the spectrum is formed primarily due to the recoil effect. This effect distorts the high energy cut-off from the shape characteristic for thermal spectra, as we illustrate in this section.

Due to a non-local nature of Comptonization, analysis of formation of Comptonization spectra in a curved space-time is a very complex issue. Below we apply a simplified treatment to derive spectra of consecutive scatterings of soft seed photons off thermal electrons, with $kT_e = 80$ keV, which are in circular motion corresponding to model A. We assume that all scatterings take place in a fixed point ($r = 1.4$ and $\theta = 0.45\pi$) and that in each scattering photons impinge from the same direction, given by $\phi_{\text{ln}} = \pi$ and $\mu_{\text{ln}} = 0$. For each photon its initial energy, E_{inf} , is generated from a blackbody distribution with $kT_{\text{bb}} = 100$ eV. Then, the following steps are repeated to simulate four subsequent scatterings of this photon:

- (i) rest energy is found [equations (10) and (11)] - the assumed initial direction yields $E_{\text{rest}} = 6E_{\text{inf}}$;
- (ii) simulation of Compton scattering in the rest frame is performed;
- (iii) energy of scattered photon, E_{inf} , is found and equations of motion are solved; photons escaping to infinity contribute to spectrum of given scattering order.

Figs. 7 and 8 show spectra at infinity and in the rest frame, respectively, for second and fourth scattering orders.

The above procedure roughly approximates effects of photon transfer in the Kerr metric. Step (i) accounts for significant blueshifts experienced by photons in the immediate vicinity of the event horizon. In turn, the assumed initial direction accounts for the fact that bending of photon trajectories results in very anisotropic radiation field close to a black hole. In simulations including full treatment of photon propagation, presented in Section 4, we find that initial directions of photons scattered close to the event horizon are

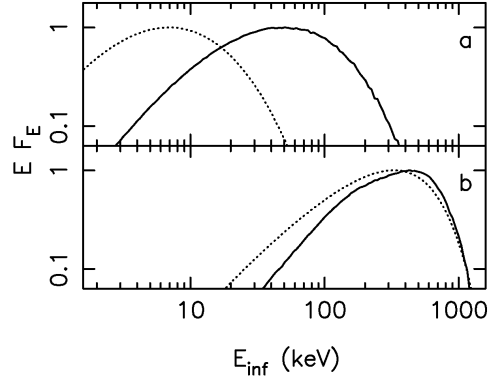


Figure 7. Solid curves show spectra emerging from second (a) and fourth (b) scattering order, observed by a distant observer at $\mu_{\text{obs}} = 0.55$. Scatterings take place at $r = 1.4$ and $\theta = 0.45\pi$ (see text for details). Dotted curves show spectra, as a function of photon energy at infinity, before scattering. All the spectra are normalized to unity in maximum.

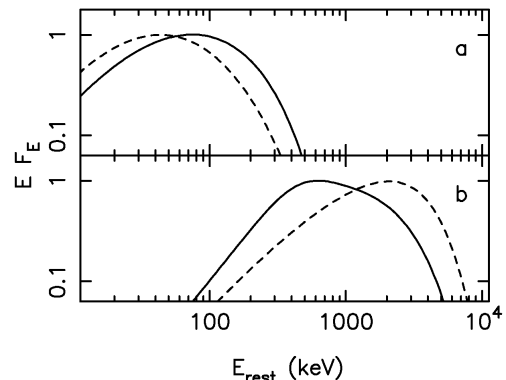


Figure 8. Figure illustrates increasing role of the recoil effect in formation of spectra emerging from higher scattering orders. Solid curves show angle-averaged spectra, in the rest frame, of photons emerging in second (a) and fourth (b) scattering order. Dashed curves show spectra of photons before scattering.

concentrated along the inward radial direction (given by the assumed values of ϕ_{ln} and μ_{ln}).

This anisotropic illumination is not important in formation of spectra emerging from lower scattering orders, for which the change of photon energies in the rest frame is dominated by energy gain from Doppler effect. In such case, photons scattered in various directions have similar spectra and the relativistic effects result in only a slight redshift and smearing of the observed spectrum. On the other hand, for higher scattering orders the angular distribution of illuminating photons becomes important, as spectra formed due to the recoil effect depend on the scattering angle and then photons scattered into various directions are subjected to different transfer effects, as described below.

Due to high initial blueshift and moderate redshifts of photons escaping after scattering (typical redshift of escaping photons is $0.5 < g < 1$), in lower scattering orders photon energies, E_{inf} , amplify by a large factor with each scattering [see Fig. 7(a)], even though in the rest frame the fractional energy transfer is small [Fig. 8(a)].

In higher scattering orders photons lose energy, in the

rest frame, forming spectrum shown by the solid curve on Fig. 8(b). Spectrum of photons observed by a distant observer [solid curve on Fig. 7(b)] is also affected by effects of photon transfer in the Kerr space-time. In particular, scattered photons with $E_{\text{rest}} > 1$ MeV emerge from forward scatterings and they weakly contribute to the observed spectrum as most of them are captured by the black hole. Photons observed with $E_{\text{inf}} < 200$ keV come from backward scatterings and they are additionally redshifted by $g \lesssim 0.5$.

The recoil and transfer effects give rise to spectrum distorted from the typical thermal shape, specifically, a flattened part occurs between 200 and 400 keV in the spectrum on Fig. 7(b). Contribution of higher scattering orders to Comptonization spectra should result in similar distortion of the high energy cut-off, although decreased scattering probability resulting from the (necessarily high) blueshift diminishes contribution of photons scattered in this regime. Spectral breaks due to this effect are indeed seen in spectra on Fig. 9(a) above 100 keV.

4 THERMAL COMPTONIZATION SPECTRA

Emergent spectra are shown in Figs. 9, 10 and 12-15. Each figure presents spectra for three inclinations, $\mu_{\text{obs}} = 0.85, 0.55$ and 0.15 . The spectra have been obtained for stellar mass, $M = 10M_{\odot}$, and supermassive, $M = 10^7M_{\odot}$, black holes. For a stellar black hole we assume a distance of $d = 5$ kpc and for a supermassive one $d = 5$ Mpc. All models assume a maximally rotating black hole and $\dot{m} = 0.5$. Unless specified otherwise, we assume that corona is spherical (model A) and that the electron temperature $kT_e = 80$ keV. Motivated by results of the previous section we focus on models with coronae located within a few gravitational radii.

4.1 Inner corona

Figs. 9 and 10 show spectra of models with a hot inner corona replacing the disc within $r_{\text{tr}} = 2$ and 4 . We assume values of the rest density yielding a similar Thomson optical depth of the corona in both cases (see Fig. 1), namely $\hat{n} = 0.4$ for $r_{\text{tr}} = 2$ and $\hat{n} = 0.2$ for $r_{\text{tr}} = 4$. Two main spectral components, emitted by the accretion flow, are shown separately. Thermal emission of the outer disc, for the assumed \dot{m} , has a peak around 0.1 keV and at a few keV for $M = 10^7M_{\odot}$ and $10M_{\odot}$, respectively. Comptonization spectra emerging in models with $r_{\text{tr}} = 2$ and 4 differ significantly, although the hot plasma parameters are similar.

For $r_{\text{tr}} = 2$ virtually bulk of Comptonized radiation comes from the ergosphere. The luminosity, slope and cut-off energy of the spectrum strongly depend on the inclination of the line of sight. This is an obvious consequence of bending to the equatorial plane, affecting trajectories of photons emerging from the ergosphere (see Fig. 5).

For photons observed close to the disc plane amplification of energy in the first scattering is so large that their energies significantly exceed the energy of disc photons. As a result, a low energy cut-off of a Comptonization spectrum may be clearly visible in the total spectrum [e.g., note deficit of photons below 1 keV in the spectrum for $\mu_{\text{obs}} = 0.15$ on Fig. 9(a)].

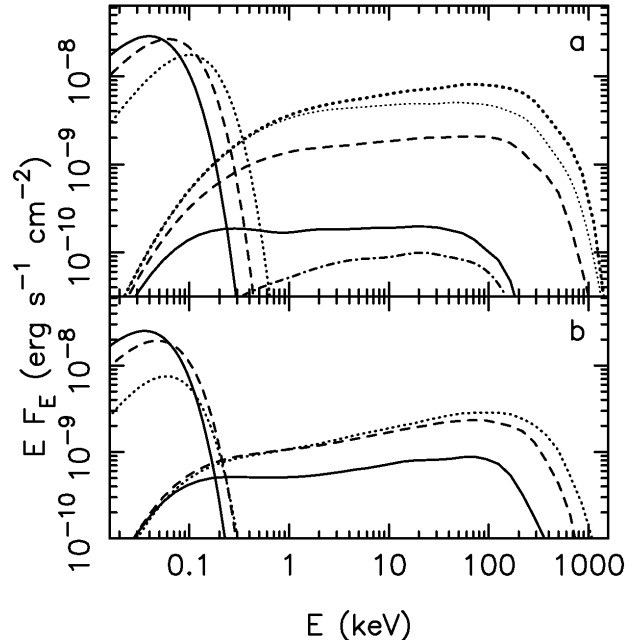


Figure 9. Spectra emerging from a hot inner corona surrounded by a cold accretion disc. The model assumes a maximally rotating black hole with a mass $M = 10^7M_{\odot}$, at a distance of $d = 5$ Mpc, accreting at $\dot{m} = 0.5$. A uniform, spherical (model A, see Section 2.1) and isothermal ($kT_e = 80$ keV) corona is assumed to replace the disc within $r_{\text{tr}} = 2$ (a) and 4 (b). The rest density $\hat{n} = 0.4$ and 0.2 for $r_{\text{tr}} = 2$ and 4 , respectively. The spectrum of thermal emission from the cold disc and the Comptonized component are shown separately. Solid, dashed and dotted curves correspond to $\mu_{\text{obs}} = 0.85, 0.55$ and 0.15 , respectively. The dot-dashed curve in Fig. 9(a) shows contribution, to spectrum observed at $\mu_{\text{obs}} = 0.85$, of photons which experienced scattering inside $r = 1.4$. The thinner dotted curve in Fig. 9(a) shows spectrum for $r_{\text{min}} = 1.23$ (see Section 2.1).

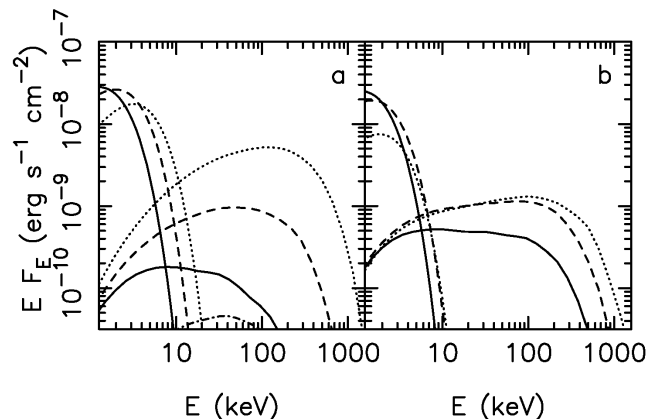


Figure 10. Same as in Fig. 9 but with $M = 10M_{\odot}$ and $d = 5$ kpc.

The supermassive and stellar black hole models produce slightly different spectra in the hard X-ray range. This property is not obvious as in our model a change of M affects directly only the temperature of the outer disk and hence the seed photons energy. The dependence of hard X-ray spectra on black hole mass is due to the fact that photon trans-

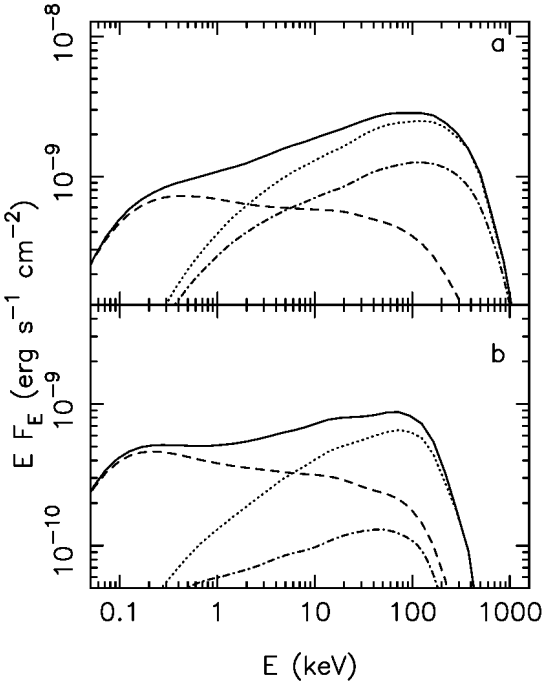


Figure 11. Solid curves show the Comptonization spectra of a model with $M = 10^7 M_{\odot}$ and $r_{\text{tr}} = 4$ [same as in Fig. 9(b)] for $\mu_{\text{obs}} = 0.15$ (a) and 0.85 (b). Dotted and dashed curves show contributions of photons which experienced at least one scattering in the ergosphere and photons scattered only outside the ergosphere, respectively. Dot-dashed curves show contribution of photons for which the last scattering took place in the ergosphere.

fer in the corona is affected by gravitational energy shifts (see Section 2.2). As a result, the corona is optically thin ($\tau \lesssim 0.5$) for photons with energies of a few tens of keV, emerging from the first scattering order in the stellar black hole model, but it is moderately thick ($\tau \gtrsim 1$) for photons below 10 keV, which arise from first few orders of scattering in the supermassive black hole model. Therefore, higher energy density of the radiation field establishes in the innermost region (where photons achieve highest energies due to gravitational effects) of the corona surrounding a supermassive black hole. Contribution of high energy photons generated in this region results in the shape of the high energy cut-off corresponding to the predominant role of the recoil effect (Section 3.3) in the model with $M = 10^7 M_{\odot}$. Also, stronger contribution of photons upscattered in the innermost region [shown by dot-dashed curves on Figs. 9(a) and 10(a)], but then scattered in the outer region of the ergosphere into directions corresponding to low inclination, results in harder spectra (above a few tens of keV) observed at $\mu_{\text{obs}} = 0.85$ in the model with $M = 10^7 M_{\odot}$.

For $r_{\text{tr}} = 4$ most scatterings take place in a region where standard thermal Comptonization effects dominate. However, the slope and luminosity of the Comptonization component remain strongly dependent on inclination. This anisotropy is entirely caused by different magnitude of the contribution of radiation produced in the ergosphere to spectra observed from various directions (see Fig. 11). Photons which do not undergo scatterings in the ergosphere form spectra with the photon spectral index $\Gamma(1-80 \text{ keV}) \approx 2.1$. A spectrum with such Γ would result from thermal Com-

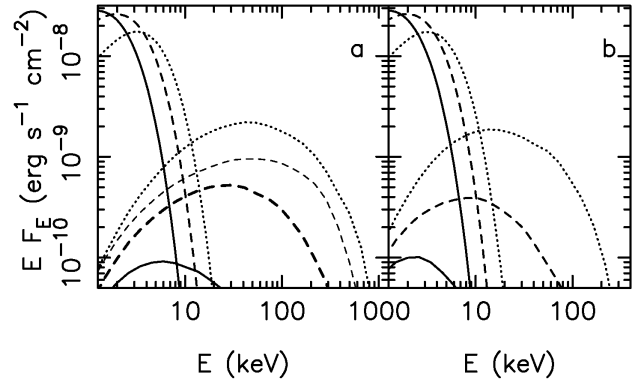


Figure 12. Dependence of Comptonization spectra on the hot plasma parameters in a model with $r_{\text{tr}} = 2$ and $M = 10M_{\odot}$. The model parameters, except for \hat{n} and kT_e , have the same values as in Fig. 10(a). (a) $\hat{n} = 0.2$, $kT_e = 80 \text{ keV}$; for a comparison, Comptonization spectrum with $\hat{n} = 0.4$ [same as in Fig. 10(a)], for $\mu_{\text{obs}} = 0.55$, is shown by the thinner dashed curve (b) $\hat{n} = 0.4$, $kT_e = 10 \text{ keV}$.

tonization, with $kT_e = 80 \text{ keV}$ and $\tau = 0.8 (= \hat{n} r_{\text{tr}})$, in flat space-time. This supports our conclusion that the only remarkable influence of the space-time metric on the Comptonization spectrum occurs for radiation emerging from the ergosphere.

Note also that ergospheric emission is significantly isotropized due to scattering in the outer regions of the corona. Therefore, contribution of radiation from the ergosphere to spectrum observed at $\mu_{\text{obs}} = 0.85$ is significant in model with $r_{\text{tr}} = 4$, although photons escaping directly from the ergosphere contribute negligibly to this spectrum.

As noted in Section 2.2, a spectral curvature may occur at a few tens of keV due to the decline of the Klein-Nishina cross-section. Indeed, a spectral break between 10 and 20 keV, related to this effect, is seen on Fig. 11(b). Furthermore, emission from the ergosphere has a significantly harder spectrum than emission from the outer regions and their superposition may result in an upturn of the spectrum, such as seen on Fig. 11(b) around 1 keV. Then, a power-law approximation of the Comptonization spectrum may be not adequate for some regions of the parameter space.

Our model does not involve an explicit description of the corona heating mechanism. However, the energy transferred to photons, measured in the corona rest frame, determines spatial distribution of heating needed to maintain the assumed uniform distribution of temperature. In particular, models with $r_{\text{tr}} = 4$ require that around 40 per cent of the heating power should be provided to the plasma within the ergosphere. Roughly 30 per cent of this energy is lost due to capturing of photons by the black hole. However, photons upscattered within the ergosphere give a major contribution to the total luminosity of Comptonized radiation, ranging from 50 per cent at low inclinations to over 70 per cent in radiation observed edge-on.

Hardening of the Comptonization component, with increasing inclination, is accompanied by weakening of the disc component. Thermal emission from the innermost region of the disc, within several R_g , is gravitationally focused to directions close to the equatorial plane (Cunningham 1975; due to this effect, emission from the disc truncated at $r_{\text{tr}} = 2$

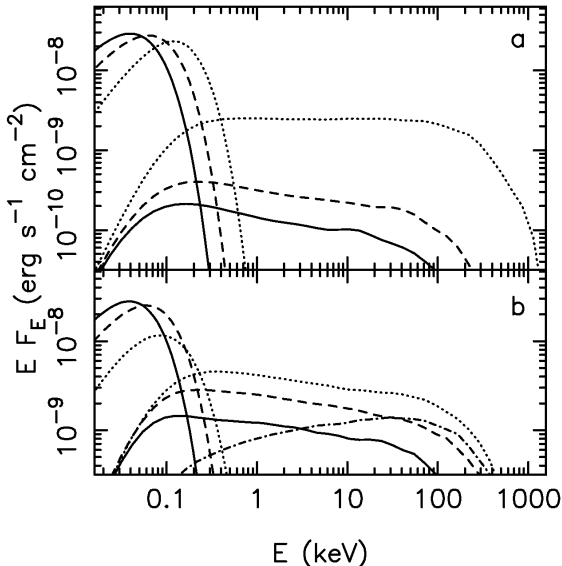


Figure 13. Spectra emerging from a spherical corona (model A) surrounding the innermost disk surface with (a) $r_c = 2$ and $\hat{n} = 0.4$; (b) $r_c = 4$ and $\hat{n} = 0.2$. Other parameters have values indicated in Fig. 9. The dot-dashed curve on Fig. 13(b) shows contribution of photons scattered in the ergosphere to spectrum observed at $\mu_{\text{obs}} = 0.15$.

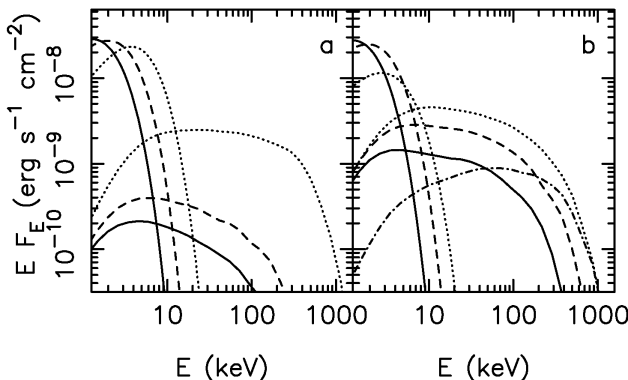


Figure 14. Same as in Fig. 13 but with $M = 10M_\odot$ and $d = 5$ kpc.

is much stronger, at high inclinations, than emission from the disc with $r_{\text{tr}} = 4$, see Figs. 9 and 10). However, angular distribution of emission from more distant regions of the disc is mostly due to the reduction of the projected area, with the observed flux given by $F_{\text{obs}} \propto \mu_{\text{obs}}$ at $r \gg 1$. Then, the ratio of the Comptonization component to the disc emission luminosities changes strongly with inclination. E.g., for $r_{\text{tr}} = 2$ the Comptonization component contributes 65 per cent to the total luminosity at $\mu_{\text{obs}} = 0.15$ but only 5 per cent at $\mu_{\text{obs}} = 0.85$.

Fig. 12 illustrates dependence of the spectrum of ergospheric emission on electron temperature and rest density in the corona. Remarkably, a relatively cold plasma ($kT_e = 10$ keV) is able to produce spectra extending beyond 100 keV, especially at high inclinations [see Fig. 12(b)].

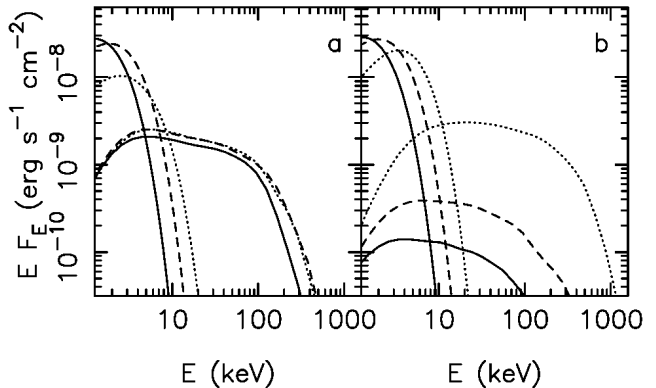


Figure 15. (a) Same as in Fig. 14(b) ($r_c = 4$) but for a non-rotating spherical corona (model B). (b) Similar as in Fig. 14(a) ($r_c = 2$) but for a corona described by model C with $\hat{n} = 4/r$.

4.2 Corona above the disc surface

Figs. 13 and 14 show spectra of models involving an optically thick disc extending down to the event horizon, with a spherical corona surrounding the disc surface within $r_c = 2$ and 4. The parameters of the corona are similar to these assumed above for the inner corona models, namely $\hat{n} = 0.4$ for $r_c = 2$ and $\hat{n} = 0.2$ for $r_c = 4$; $kT_e = 80$ keV. The innermost disc immersed in the corona provides a very strong supply of seed photons. However, the Comptonization spectra are softer than spectra emerging from inner coronae with the same parameters, which is due to the fact that majority of photons upscattered in the ergosphere is absorbed by the disc [see Fig. 5(c)(d)].

In models with $r_c = 4$ the Comptonization spectra are dominated by emission from regions outside the ergosphere and similar slopes characterize spectra observed from various directions. The ergospheric component [shown on Figs. 13(b) and 14(b)] contributes up to 25 per cent to the luminosity of Comptonization radiation. However, luminosity and cut-off energies of the spectra increase for higher inclinations, which is due to the circular motion of the corona.

To confirm this last conclusion we show on Fig. 15(a) spectrum of a non-rotating corona (model B). The Comptonization spectra are again dominated by emission generated outside the ergosphere, which is weakly affected by the ray bending or gravitational shifts of energies. As a result, anisotropy of the Comptonization component is negligible.

Finally, we consider sensitiveness of the properties of ergospheric Comptonization spectra on angular velocity distribution in a corona. Fig. 15(b) shows spectra emerging from a corona described by model C with $\hat{n} = 4/r$. The corona fills a region within 12° of the disc plane and covers the disc surface within $r_c = 2$. In this model all scatterings take place close to the equatorial plane in a plasma rotating with $V \approx 0.6$, which results in slightly different angular distribution of Comptonized photons with respect to the spherical corona model. In the latter model a large number scatterings take place in a slowly rotating plasma at high latitudes. However, the basic properties of the spectra appear not affected by the change of velocity field and geometrical shape of the corona.

5 DISCUSSION

5.1 Comparison with similar studies

The first study of the impact of the Kerr metric on spectra generated by a black hole accretion flow was performed by Cunningham (1975). He pointed out that most of the thermal emission from innermost regions of a disc lying in the equatorial plane is gravitationally focused into directions close to the disc plane. We find that a similar focusing affects also radiation arising from Comptonization in the vicinity of a Kerr black hole.

Piran & Shaham (1977a,b) investigated Compton scattering in the Kerr metric. They pointed out Compton scattering, taking place in the ergosphere, as the most astrophysically feasible Penrose process. As an application of such processes they considered production of γ -rays by a hot plasma in the ergosphere.

As we discuss in Section 3, the gravitational effects may indeed significantly increase the energy of a photon scattered in the ergosphere. However, probability of the most efficient processes is extremely low and they appear not important for formation of spectra. Piran & Shaham (1977b) point out dependence of the emerging spectra on observer's inclination, in agreement with our results. On the other hand, they concluded that thermal Comptonization in the ergosphere gives rise to spectra with a power-law shape extending into MeV range without any exponential-like cut-off. We do not confirm this last conclusion as our spectra, derived for similar electron temperatures, have generic thermal-like cut-offs. We suspect that this discrepancy results from a rather poor statistical quality of spectra presented by Piran & Shaham (1977b). Their spectra were obtained with a typical number of 10^3 photons. On the other hand, we find that at least 10^6 photons scattered in a corona is needed in a simulation to correctly derive the high energy part of angle-averaged spectrum.

Thermal Comptonization in two-temperature advection-dominated flows in the Kerr metric was studied by Kurpiewski & Jaroszyński (1999) and Manmoto (2000). However, their models assumed a hot flow extending out to $\sim 1000R_g$. Therefore, their spectra arise mostly due to thermal processes taking place far from a black hole, where gravitational field is not important for radiative processes. Then, these authors did not notice any direct impact of the gravitational field metric on a Compton effect. A weak dependence of their spectra on the black hole spin parameter is due to changes in velocity field, density and electron temperature profiles of the accretion flow.

5.2 Applicability to black hole systems

Clearly, effects considered in this paper are important for the emerging spectra only if a substantial part of hard X-rays comes from the ergosphere. On theoretical ground, scenario with strong emission from the ergosphere, in case of accretion onto a rapidly rotating black hole, is supported by preliminary results of general relativistic MHD simulations (see below) as well as by the standard theory of Keplerian α -discs. The latter predicts that 17 per cent of the gravitational power is dissipated within the ergosphere (for $a = 0.998$). This implies that significant emission of hard X-rays from

the ergosphere can be expected in models which assume that strong release of the accretion energy occurs in a corona surrounding the disc. Although details of the heat deposition (presumably involving buoyancy and reconnection of magnetic fields) are uncertain, the spatial distribution of the heating is most likely to follow the dissipation distribution in the disc.

Simulations of accretion driven by turbulent stresses generated by the magnetorotational instability (e.g. Hawley & Balbus 2002; De Villiers et al. 2003) support a model with an inner corona formed within a few gravitational radii. These simulations commonly indicate formation of a hot inner torus, of the size slightly exceeding r_{rms} , at the inner edge of a nearly Keplerian disc. For a rapidly rotating black hole the inner torus, which can be plausibly related to coronal activity of the inner region, is located mainly within the ergospheric region.

Observations of black hole systems indicate that at high accretion rates geometry of the innermost region is similar to that considered in this paper. High temperature of thermal component, dominating the soft-state spectra of black hole binaries, implies disc extending down close to a black hole (e.g. Gierliński & Done 2004). A similar conclusion comes from the amount of X-rays reflected from the disc in a Seyfert galaxy, MCG-6-30-15 (Lee et al. 1999), which seems to be a high accretion rate object (Nowak & Chiang 2000). Furthermore, Fe K α line profiles indicate a very central location of the hard X-ray source in high accretion rate objects, including XTE J1650-500 (Miller et al. 2002) and GX 339-4 (Miller et al. 2004) in their soft states as well as MCG-6-30-15 (Wilms et al. 2001). In our subsequent paper we find that relativistic line profiles observed in black hole systems can be explained in a model involving illumination of a disc by a central corona and that the extreme profiles noted above require such a corona to be constrained within the ergosphere.

Given the above observational evidence, we expect that results of this paper should be relevant to modeling observations of objects with high luminosity to Eddington luminosity ratio. On the other hand, we emphasize that nonthermal tails observed in some soft state spectra (e.g. McConnell et al. 2002) cannot be due to special or general relativistic effects in a thermal plasma. Such a tail most likely indicates that Comptonizing plasma contains nonthermal (in addition to thermalized) electrons (e.g. Zdziarski 2000), which has not been taken into account in this study.

Observations in lower luminosity states, including most normal Seyfert 1 galaxies and black hole binaries in their hard states, require that the innermost part of accretion disc is replaced by an optically thin flow, with the optically thick material extending down only to $20 - 50R_g$ (e.g. Done, Madejski, Życki 2000; Miller et al. 2001; Życki, Done & Smith 1998; 1999). Hard X-ray spectra of such objects are well fitted by thermal Comptonization models, usually using a uniform temperature and density distribution, with electron temperature within 50-100 keV and a Thomson optical depth close to unity (e.g. Zdziarski 2000). If the spacial extent of such a uniform, hot plasma corresponds to the distance of truncation of the disc, then the relativistic effects considered in this paper should not be important for the spectra.

However, if the plasma is heated due to dissipation of

gravitational energy in a hot inner flow around a rotating black hole, then enhanced emission from the innermost regions can be expected. Accretion flows around rapidly rotating black holes release a large fraction of the gravitational power within the ergosphere, as noted above. Furthermore, advection increases electron temperature in the innermost region of optically thin flows (Esin et al. 1997). Then, emission of an inner corona may be very centrally concentrated and a detailed modeling is required to check importance of the gravitational effects for formation of spectra in such a case.

Finally, we indicate that hints for orientation-dependent hard X-ray spectra, consistent with predictions of our model, come from recent studies of X-ray observations of Seyfert galaxies. In their analysis of OSSE observations, Zdziarski, Poutanen & Johnson (2000) found that Seyfert 2 galaxies have significantly harder spectra than Seyfert 1s, with the average photon spectral index, in the 50 - 200 keV range, being approximately 2 and 2.5, respectively. As only in one Seyfert 2, considered in that paper, absorption of X-rays is Thomson thick, this result may indicate an intrinsic difference between the hard X-ray spectra of Seyfert 1s and 2s. A similar conclusion comes from *BeppoSAX* observations (Deluit & Courvoisier 2003), which indicate also that the cut-off energy is higher in Seyfert 2s than in Seyfert 1s.

According to the unification model of active galactic nuclei (e.g. Antonucci 1993) the difference between type 1 and type 2 galaxies is only due to the viewing angle. Namely, the same object would be classified as a Seyfert 1 or as a Seyfert 2 when observed at low and high inclinations, respectively. Following this unification scheme, we indicate that Seyfert 2 galaxies may indeed be intrinsically harder than Seyfert 1s due to gravitational focusing of X-rays by rotating black holes.

6 SUMMARY

We have developed the Monte Carlo model for studying Comptonization spectra emerging from accretion flows in the Kerr metric. We find that strong gravity effects are crucial for the formation of the spectra only in the ergosphere of a rotating black hole. Spectra involving a significant contribution from the ergosphere are strongly dependent on the observer's inclination. Furthermore, intrinsic curvature and spectral breaks, related to strong gravity effects, may occur.

The high energy part of the ergospheric Comptonization spectrum is significantly attenuated when optically thick material is present in the equatorial plane of the Kerr geometry. Therefore, a noticeable Comptonization radiation from the ergosphere is more likely in models with a tenuous plasma occupying the innermost region.

We indicate that hardening of Comptonization spectra with increasing inclination, which is predicted by Comptonization in the Kerr metric, can be considered as an explanation for the difference between the hard X-ray spectra of Seyfert 1 and Seyfert 2 galaxies.

ACKNOWLEDGMENTS

This research has been supported by grants from Polish Committee for Scientific Research (PBZ-KBN-054/P03/2001) and from Łódź University. I am grateful to Włodek Bednarek for his encouragement and to Marek Sikora and prof. Maria Giller for their comments. I also thank the referee for very careful reading of the manuscript and for valuable suggestions.

REFERENCES

Antonucci R., 1993, ARA&A, 31, 473
 Bardeen J. M., Cunningham C. T., 1973, ApJ, 183, 237
 Bardeen J. M., Press W. H., Teukolsky S. A., 1972, ApJ, 178, 347
 Chakrabarti S., Titarchuk L., 1995, ApJ, 455, 623
 Cunningham C. T., 1975, ApJ, 202, 788
 De Villiers J.-P., Hawley J. F., Krolik J. H., 2003, ApJ, 599, 1238
 Deluit S., Courvoisier T., 2003, A&A, 399, 77
 Done C., Madejski G., Życki P., 2000, ApJ, 536, 213
 Esin A. A., McClintock J.E., Narayan R., 1997, ApJ, 489, 865
 Gierliński M., Done C., 2004, MNRAS, 347, 885
 Gierliński M., Maciołek-Niedźwiecki A., Ebisawa K., 2001, MNRAS, 325, 1253
 George I. M., Fabian A. C., 1991, MNRAS, 249, 352
 Górecki A., Wilczewski W., 1984, Acta Astronomica, 34, 141
 Haardt F., Maraschi L., 1991, ApJ, 380, L51
 Hawley J. F., Balbus S. A., 2002, ApJ, 573, 738
 Kurpiewski A., Jaroszynski M., 1999, A&A, 346, 713
 Laurent P., Titarchuk L., 1999, ApJ, 511, 289
 Laor A., Netzer H., Piran T., 1990, MNRAS, 242, 560
 Lee J., Fabian A., Brandt W., Reynolds C., Iwasawa K., 1999, MNRAS, 310, 973
 Liang E. P., Price R. H., 1977, ApJ, 218, 247
 Manmoto T., 2000, ApJ, 534, 734
 McConnell M. L. et al., 2002, ApJ, 572, 984
 Miller J. M. et al., 2001, ApJ, 546, 1055
 Miller J. M. et al., 2002, ApJ, 570, L69
 Miller J. M. et al., 2004, ApJL, in press (astro-ph/0312033)
 Narayan R., Yi I., 1995, ApJ, 452, 710
 Novikov I. D., Thorne K. S., 1973, in Black Holes, ed. C. De Witt & B. De Witt (New York: Gordon & Breach), 343
 Nowak M., Chiang J., 2000, ApJ, 531, L13
 Page D., Thorne K. S., 1974, ApJ, 191, 499
 Piran T., Shaham J., 1977a, Physical Review, 16, 1615
 Piran T., Shaham J., 1977b, ApJ, 214, 268
 Popham R., Gammie C. F., 1998, ApJ, 504, 419
 Shapiro S. L., Lightman A. P., Eardley D. M., 1976, ApJ, 204, 187
 Thorne K. S., 1974, ApJ, 191, 507
 Wilms J., Reynolds C. S., Begelman M. C., Reeves J., Molendi S., Staubert R., Kendziorra E., 2001, MNRAS, 328, L27
 Zdziarski A. A., 2000, in IAU Symp. 195, Highly Energetic Physical Processes and Mechanisms for Emission from Astrophysical Plasmas, ed. P. C. H. Martens, S. Tsuruta & M. A. Weber (San Francisco: ASP), 153
 Zdziarski A. A., Poutanen J., Johnson W. N., 2000, ApJ, 542, 703
 Życki P., Done C., Smith D., 1998, ApJ, 496, L25
 Życki P., Done C., Smith D., 1999, MNRAS, 305, 231